Available online at www.sciencedirect.com
ScienceDirect
Journal of Sound and Vibration 303 (2007) 741–752
JOURNAL OF SOUND AND VIBRATION
www.elsevier.com/locate/jsvi

# A model of acoustic impedance of perforated plates with bias flow considering the interaction effect

Seong-Hyun Lee[a], Jeong-Guon Ih[a,*], Keith S. Peat[b]

[a]*Center for Noise and Vibration Control, Department of Mechanical Engineering, Korea Advanced Institute of Science and Technology (KAIST), Science Town, Daejeon 305-701, Korea*
[b]*Department of Aeronautical and Automotive Engineering, Loughborough University, Loughborough, Leicestershire LE11 3TU, UK*

Received 25 January 2006; received in revised form 24 January 2007; accepted 3 February 2007
Available online 27 March 2007

**Abstract**

A numerical model of the acoustic impedance of perforated plates under bias flow conditions was derived, with consideration given to the interaction effect between orifices. The normalized impedance divided by the mean flow Mach number of an orifice was expressed as a function of the Strouhal number varying the porosity and thickness-to-radius ratio. The prediction model was accomplished by solving the incompressible Euler equation for an orifice in a finite-thickness partition that spans a tube. The acoustic impedance was also measured experimentally using an error-controlled setup. As porosity increased, the reactance tended to decrease because the attached mass on the orifices is decreased by the interaction effect. The acoustic impedance predicted by the proposed model shows reasonable agreement with measured data over the wide range of porosity values tested, except where nonlinear effects are observed. For comparison of the performance of the new impedance model against two previous models that did not consider the interaction effect, each was used in the evaluation of the transmission loss of perforated baffles. The predicted transmission losses using the new impedance model agree better with the measured data than those using the previous models, in particular at high porosities and at high frequencies.


## 1. Introduction

Perforated plates under bias flow, or cross-flow, are widely used in automotive mufflers and flow ducts of combustion systems for the suppression of noise and flow instability. Noise attenuation occurs due to impedance mismatch and energy dissipation at orifices as well as within backing porous materials, where present. In these cases, the acoustical performance of perforated plates contributes greatly to the noise characteristics of a whole system. The flow through the orifice and the interaction with the surrounding tube wall and other orifices affect substantially the acoustic impedance. Therefore, a realistic model is needed for the characterization of the acoustic impedance of orifices under bias flow condition, to enable the overall prediction of the acoustic performance of a silencer system.

*Corresponding author. Tel.: +82 42 869 3035; fax: +82 42 869 8220.
*E-mail address:* J.G.Ih@kaist.ac.kr (J.-G. Ih).

0022-460X/$ - see front matter © 2007 Elsevier Ltd. All rights reserved.
doi:10.1016/j.jsv.2007.02.001

The acoustic properties of perforated plates under bias flow condition have been studied theoretically and experimentally by many researchers. Bauer [1] introduced the effect of bias flow velocity on the acoustic impedance model of perforated liner with grazing flow. Howe [2] theoretically derived the Rayleigh conductivity of an orifice located on an infinite plate baffle with infinitesimal thickness under bias flow condition. A sufficiently large Reynolds number was assumed such that the viscous effect was deemed negligible except near the rim of an orifice. Bechert [3] showed that the existence of the Kutta condition at the edge of a rigid surface in a flow causes the shedding of fluctuating vorticity and this process leads to sound absorption by extracting energy from the sound field. Hughes and Dowling [4] expanded Howe's model [2] to a very thin perforated screen backed by a rigid wall, on which orifices are distributed very sparsely. Good agreement between predicted and experimental results was observed. Howe [5] showed that the acoustic properties of a perforated liner under grazing flow conditions can be changed by varying the orifice thickness. Peat et al. [6] analytically investigated the effect of finite thickness upon the acoustic impedance of a rectangular aperture in a plate with grazing flow. Jing and Sun [7] modified Howe's model [2] to consider the thickness effect by using an oscillating air mass piston model, which was first used by Rayleigh [8] in the absence of flow. Later, Jing and Sun [9] solved the governing equation derived by Howe [2] numerically, using the boundary-element method with consideration of the thickness. Bellucci et al. [10] presented a model to predict the acoustic impedance of a perforated screen. They combined two different sub-models for revealing the linear and nonlinear impedance behavior. Eldredge and Dowling [11] investigated the effects of a perforated liner with mean bias flow on the absorption of planar acoustic waves in a circular duct. Several experimental works were carried out with bias flow through a perforated screen. Dean and Tester [12] showed experimentally that the acoustic impedance can be controlled by changing the bias flow velocity. The experiments of Salikuddin et al. [13] showed that the resistance of a perforated plate increases and the reactance decreases with increasing bias mean flow. Jing and Sun [7] showed that the absorption coefficient and effective bandwidth of a perforated liner increase as the bias flow velocity increases and also that the plate thickness plays a dominant role in the acoustic properties.

Previous researchers assumed that the acoustic impedance of perforated plates can be derived from the impedance of a single orifice in an infinite plate baffle, given the assumption that the spacing between orifices is much larger than the radius of an orifice. However, in practical applications, the orifices are usually closely spaced, such that interactions between neighboring orifices can influence the acoustic performance of perforated liners profoundly. Due to this reason, there has been a limitation in actual applications of previous orifice impedance models. Ingard [14] considered the two-aperture interaction case and he found that the end correction was very dependent on the separation. Fok [15] investigated the interaction effects between orifices in the absence of flow by considering the conductance of an aperture in a partition across a tube. Melling [16] summarized the impedance models and suggested an impedance model of a perforate considering the interaction effects by using Fok's function [15]. Those models for the interaction effect are only applicable to the orifices with infinitesimal thickness and no mean flow condition. In this research, the acoustic impedance of a perforated circular orifice with bias flow is analyzed numerically and experimentally considering the interaction between orifices. The numerical prediction was accomplished by solving the incompressible Euler equation for an orifice in a finite-thickness partition that spans a circular tube. The interaction effect was considered by varying the radius ratio of orifice to tube. The acoustic impedance was measured under very carefully controlled measurement conditions for varying values of the parameters of influence. These key parameters are the orifice diameter, orifice thickness, plate porosity and mean flow Mach number through an orifice. To verify the effect of interaction between orifices, the transmission loss of perforated baffles under bias flow condition was also measured and predicted.

## 2. Theoretical analysis

The acoustic impedance of perforated liners, with consideration given to the interaction effects, can be analyzed by using an approximate method that employs the geometry of an orifice in a finite-thickness partition that spans a circular cylindrical tube, as illustrated in Fig. 1 in which the cylindrical coordinate $(x, r, \theta)$ is used. The tube wall influences both the streamline and the kinetic energy of oscillating mass through an orifice, so the impedance of an orifice in a finite-thickness partition across a tube differs from that of an

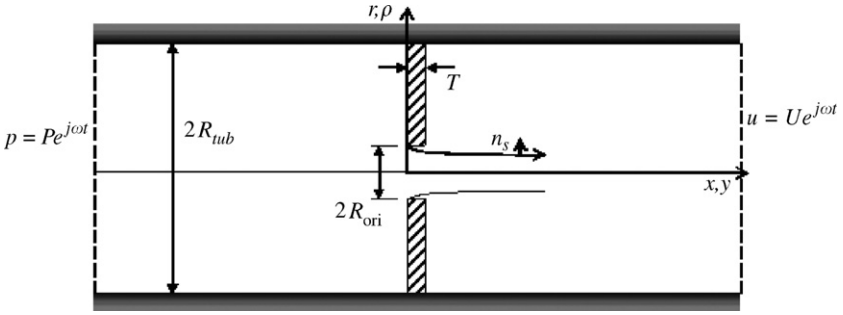


Fig. 1. Orifice in a thick partition within a circular tube with steady bias flow.

orifice in an infinite baffle. If the radius ratio of orifice to tube, $R_{\text{ori}}/R_{\text{tub}}$, becomes zero, the orifice can be assumed to be located in an infinite baffle. Uniform harmonic pressure and velocity perturbations are considered at the inlet and outlet of the tube as

$$p = P\mathrm{e}^{\mathrm{j}\omega t} \quad \text{(at inlet surface)}, \tag{1a}$$

$$u = U\mathrm{e}^{\mathrm{j}\omega t} \quad \text{(at outlet surface)}. \tag{1b}$$

These perturbations are assumed to be produced by a low-frequency sound wave, such that the wavelength is much larger than the orifice radius. At high Reynolds numbers, the viscous force can generally be considered as negligible in comparison with the inertia force and is expected to play a dominant role only at the rim of orifice. If the Mach number of the mean flow is low, the density is not much changed by variations in the flow velocity. So, where a low Mach number, high Reynolds number steady flow through a tube is concerned, one can use the incompressible Euler equation [2]. The viscous effect at the inlet edge of the orifice is considered by employing a Kutta condition, such that the fluctuating velocity and pressure are non-singular at the rim of the orifice. If the orifice is exposed to incompressible, inviscid fluid flows, the vorticity far from the body will be zero and the flow will be irrotational by the Kelvin's theorem [17]. Vorticity changes are therefore caused by the rotation and stretching of vortex tubes at the boundaries and diffusion across the boundaries by viscosity. To simplify the governing equations, the radial component of the perturbation vorticity is neglected under the assumption that the radial diffusion of vorticity by the shear layer is ineffective on the enthalpy through the orifice. In addition, the cross-product of mean flow velocity and vorticity can also be neglected [2]. The linearized Euler equation [2] can be written as

$$\nabla^2 h = -\nabla \cdot (\boldsymbol{\Omega} \times \boldsymbol{U}_0), \tag{2}$$

where $\boldsymbol{\Omega}$ is the perturbation vorticity, $\boldsymbol{U}_0$ the mean flow velocity through the orifice and $h$ is the Bernoulli enthalpy, defined by

$$h = \frac{p}{\rho_0} + \boldsymbol{U}_0 \cdot \boldsymbol{u} = -\frac{\partial \phi}{\partial t} + \text{const.} \tag{3}$$

Here, $\rho_0$ is the density of a medium, $\boldsymbol{u}$ is the perturbation velocity, and $\phi$ is the perturbation velocity potential. For high Reynolds number flow the shear layer becomes very thin. Thus the perturbation vorticity [2] can be approximated as

$$\boldsymbol{\Omega} = \gamma \exp\left[\mathrm{j}\omega(t - s/U_0)\right]\delta(n_s)\boldsymbol{k}, \tag{4}$$

where $\gamma$ is the strength of a shed vortex sheet, $s$ the distance from the inlet edge along the vortex streamline, $\delta(x)$ the delta function, $n_s$ the normal coordinate of free streamline of bias flow, and $\boldsymbol{k}$ the unit vector in the $\theta$ direction. From Eqs. (2) and (4), the following axisymmetric Poisson equation can be obtained:

$$\frac{1}{r}\frac{\partial}{\partial r}\left(r\frac{\partial h}{\partial r}\right) + \frac{\partial^2 h}{\partial x^2} = -\nabla \cdot \left[\gamma U_0 \exp\left(-\frac{\mathrm{j}\omega s}{U_0}\right)\delta(n_s)\boldsymbol{n}_s\right]. \tag{5}$$

Eq. (5) can be converted to the integral equations using a half-space Green function, $G_h$, which satisfies the following relations [9]:

$$\nabla^2 G_h = \delta(\boldsymbol{x}-\boldsymbol{y}), \quad \left.\frac{\partial G_h}{\partial y}\right|_{y=0} = 0, \tag{6a,b}$$

$$G_h(x,r,\theta;y,\rho,\varphi) = -\frac{1}{4\pi}\frac{1}{\sqrt{(x-y)^2+r^2+\rho^2-2r\rho\,\cos(\theta-\varphi)}} - \frac{1}{4\pi}\frac{1}{\sqrt{(x+y)^2+r^2+\rho^2-2r\rho\,\cos(\theta-\varphi)}}. \tag{7}$$

In other words, Eq. (7) can be the solution of Eq. (5) with the boundary conditions in Eqs. (6a) and (6b) in cylindrical coordinates as shown in Fig. 2. Fig. 2 shows the integration space that is divided into two regions by the surface $\Sigma 0$. Surfaces in the two domains are designated as $\Sigma_i$ $(i=1,2,\ldots,8)$. The geometry of the free streamline obtained from experimental data [18] depends upon the following nine variables [19]: $x$; $R_0$; $R_{\text{tub}}$; $U_0$; $\rho_0$; $\mu$, the dynamic viscosity; $\gamma_w$, the specific weight; $\sigma_t$, the surface tension of the liquid; $k_r$, the scale of surface roughness in the pipe. Using the Buckingham $\pi$-theorem to combine these variables into dimensionless groupings, one can obtain

$$\frac{r}{R_{\text{ori}}} = F_0\left(\frac{z}{R_{\text{ori}}}, \frac{R_{\text{ori}}}{R_{\text{tub}}}, \frac{\rho_0 U_0 R_{\text{ori}}}{\mu}, \frac{U_0}{(R_{\text{ori}}\gamma_w/\rho_0)^{1/2}}, \frac{U_0}{(\sigma_t/\rho_0 R_{\text{ori}})^{1/2}}, \frac{k_r}{R_{\text{ori}}}\right). \tag{8}$$

The last term on the right-hand side will be disregarded because the surfaces are assumed to be smooth. If the symbols *Re*, *Fr*, and *We* are used to represent the Reynolds, Froude, and Weber numbers, respectively, then the above equation becomes

$$\frac{r}{R_{\text{ori}}} = F_1\left(\frac{x}{R_{\text{ori}}}, \frac{R_{\text{ori}}}{R_{\text{tub}}}, Re, Fr, We\right). \tag{9}$$

In this study, if the viscous, gravitational, and capillary effects are assumed to be negligible, the jet profile can be determined by only the radius ratio of orifice to tube. The length of the tube in each domain, $L$, is set to $5R_{\text{tub}}$, and the length of free streamline is truncated at $5R_{\text{ori}}$. The boundary conditions for solving the governing equations are

$$\frac{\partial h}{\partial n} = 0 \quad (\text{on } \Sigma_1, \Sigma_2, \Sigma_3, \Sigma_6, \text{ and } \Sigma_8), \tag{10a}$$

$$h = H_1 \quad (\text{on } \Sigma_7), \quad \frac{\partial h}{\partial n} = H_2 \quad (\text{on } \Sigma_4). \tag{10b,c}$$

Eq. (10b) enforces a uniform sinusoidal pressure fluctuation at the inlet, $\Sigma_7$, and Eq. (10c) gives a uniform sinusoidal velocity fluctuation at the outlet, $\Sigma_4$. Finally, the expressions for $h$ in the two domains can be

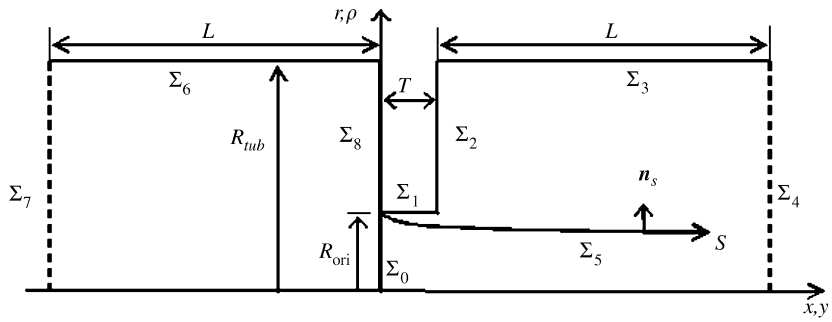


Fig. 2. Integration domains and surfaces.

obtained as

$$\frac{1}{2}h = -\int_{\Sigma_0}\frac{\partial h}{\partial y}G_h\,\mathrm{d}S - \int_{\Sigma_6} h\frac{\partial G_h}{\partial \rho}\,\mathrm{d}S - \int_{\Sigma_7}\left(\frac{\partial h}{\partial y}G_h - h\frac{\partial G_h}{\partial y}\right)\mathrm{d}S \quad (x<0) \tag{11}$$

and

$$\begin{aligned}\frac{1}{2}h = {} & \int_{\Sigma_0}\frac{\partial h}{\partial y}G_h\,\mathrm{d}S + \int_{\Sigma_1} h\frac{\partial G_h}{\partial \rho}\,\mathrm{d}S - \int_{\Sigma_2} h\frac{\partial G_h}{\partial y}\,\mathrm{d}S + \int_{\Sigma_3} h\frac{\partial G_h}{\partial \rho}\,\mathrm{d}S \\ & + \int_{\Sigma_4}\left(\frac{\partial h}{\partial y}G_h - h\frac{\partial G_h}{\partial y}\right)\mathrm{d}S - \int_{\Sigma_5}\gamma U_0\exp\left(-\frac{\mathrm{j}\omega s}{U_0}\right)\frac{\partial G_h}{\partial n_s}\,\mathrm{d}S \quad (x>0).\end{aligned} \tag{12}$$

In order to couple the two domains, the following continuity equations of Bernoulli enthalpy and its normal derivative can be used:

$$h|_{x=0_+,r} = h|_{x=0_-,r}, \quad \left.\frac{\partial h}{\partial x}\right|_{x=0_+,r} = \left.\frac{\partial h}{\partial x}\right|_{x=0_-,r}. \tag{13a,b}$$

Using Eqs. (11)–(13), the integral equations on each surface can be derived as

$$\begin{aligned}& 2\int_{\Sigma_0}\frac{\partial h}{\partial y}G_h\,\mathrm{d}S + \int_{\Sigma_1} h\frac{\partial G_h}{\partial \rho}\,\mathrm{d}S - \int_{\Sigma_2} h\frac{\partial G_h}{\partial y}\,\mathrm{d}S + \int_{\Sigma_3} h\frac{\partial G_h}{\partial \rho}\,\mathrm{d}S \\ & + \int_{\Sigma_4}\left(\frac{\partial h}{\partial y}G_h - h\frac{\partial G_h}{\partial y}\right)\mathrm{d}S + \int_{\Sigma_6} h\frac{\partial G_h}{\partial \rho}\,\mathrm{d}S + \int_{\Sigma_7}\left(\frac{\partial h}{\partial y}G_h - h\frac{\partial G_h}{\partial y}\right)\mathrm{d}S \\ & - \int_{\Sigma_5}\gamma U_0\,\exp\left(-\frac{\mathrm{j}sSt}{R_{\mathrm{ori}}}\right)\frac{\partial G_h}{\partial n_s}\,\mathrm{d}S = 0 \quad (\text{on } \Sigma_0),\end{aligned} \tag{14}$$

$$\begin{aligned}& -\frac{1}{2}h + \int_{\Sigma_0}\frac{\partial h}{\partial y}G_h\,\mathrm{d}S + \int_{\Sigma_1} h\frac{\partial G_h}{\partial \rho}\,\mathrm{d}S - \int_{\Sigma_2} h\frac{\partial G_h}{\partial y}\,\mathrm{d}S + \int_{\Sigma_3} h\frac{\partial G_h}{\partial \rho}\,\mathrm{d}S \\ & + \int_{\Sigma_4}\left(\frac{\partial h}{\partial y}G_h - h\frac{\partial G_h}{\partial y}\right)\mathrm{d}S - \int_{\Sigma_5}\gamma U_0\,\exp\left(-\frac{\mathrm{j}sSt}{R_{\mathrm{ori}}}\right)\frac{\partial G_h}{\partial n_s}\,\mathrm{d}S = 0 \quad (\text{on } \Sigma_1-\Sigma_4),\end{aligned} \tag{15}$$

$$\frac{1}{2}h + \int_{\Sigma_0}\frac{\partial h}{\partial y}G_h\,\mathrm{d}S + \int_{\Sigma_6} h\frac{\partial G_h}{\partial \rho}\,\mathrm{d}S + \int_{\Sigma_7}\left(\frac{\partial h}{\partial y}G_h - h\frac{\partial G_h}{\partial y}\right)\mathrm{d}S = 0 \quad (\text{on } \Sigma_6 \text{ and } \Sigma_7). \tag{16}$$

Here, $St'$ ( $= R_{\mathrm{ori}}\omega/U_0$) is the Strouhal number. The strength of the shed vorticity $\gamma$ is determined by the Kutta condition, which can be written as

$$\left.\frac{\partial h}{\partial n}\right|_{x=0,r=R_{\mathrm{ori}}^-} = 0, \tag{17}$$

where $n$ is normal to the separation streamline at the inlet edge of the orifice.

The integral equations (14)–(16) can be solved numerically using the boundary-element method. The surface integrals can be simplified into line integrals by using the axisymmetric potential function [20]. Constant elements are adopted and the control points on $\Sigma_0$–$\Sigma_4$, $\Sigma_6$, and $\Sigma_7$ are designated as $N_i$ ($i = 0$–4, 6, 7) for each $i$th surface. The unknown variable on $\Sigma_0$ and $\Sigma_7$ is $\partial h/\partial y$ and the unknown variable on $\Sigma_0$–$\Sigma_4$ and $\Sigma_6$ is $h$. In the last integral in Eqs. (14) and (15), the only unknown variable is the strength of the shed vortex sheet, $\gamma$. The Rayleigh conductivity is defined as the ratio of volume flux to potential difference between the ends of the channel [9]. After the numerical implementation, the Rayleigh conductivity of the total system, namely a tube and an orifice in a partition, can be obtained as

$$K_R^{\mathrm{tot}} = \frac{\mathrm{j}\omega\rho_0 Q}{p_+ - p_-} = \frac{\mathrm{j}\omega Q}{(p_+ - p_-)/\rho_0} = \frac{\mathrm{j}\omega Q}{\bar{h}_7 - \bar{h}_4}, \tag{18}$$

where $(p_+ - p_-)$ denotes the pressure difference across the total system, $\bar{h}_7$ and $\bar{h}_4$ are the Bernoulli enthalpies averaged across the inlet and outlet cross-section of the tube, respectively, and $Q$ is the volume flux, defined as

$$Q = \frac{1}{\mathrm{j}\omega}\int_{\Sigma_0}\frac{\partial h}{\partial x}\,\mathrm{d}S. \tag{19}$$

The total conductivity, which is obtained by solving the foregoing integral equations numerically, may be considered to consist of two separate parts, namely the conductivity of the tube, $K_R^{\mathrm{tub}}$, and the conductivity of an orifice in the partition, $K_R^{\mathrm{ori}}$. Then, the total conductivity, $K_R^{\mathrm{tot}}$, can be expressed as

$$\frac{1}{K_R^{\mathrm{tot}}} = \frac{1}{K_R^{\mathrm{tub}}} + \frac{1}{K_R^{\mathrm{ori}}}. \tag{20}$$

Using the theoretical conductivity value of the tube, $K_R^{\mathrm{tub}}$, which is equal to $\pi R_{\mathrm{tub}}^2/(2L+T)$, the conductivity of an orifice in a finite plate can be obtained from Eq. (20). It can be converted to the normalized acoustic impedance of an orifice as

$$Z_{\mathrm{ori}} = \frac{p_+ - p_-}{\rho_0(\omega/k)(Q/S)} = \mathrm{j}kS\frac{p_+ - p_-}{\mathrm{j}\omega\rho_0 Q} = \frac{\mathrm{j}kS}{K_R^{\mathrm{ori}}}, \tag{21}$$

where $S = \pi R_{\mathrm{ori}}^2$ and $k$ is the wavenumber. Fok [15] derived the conductivity of an orifice using both thickness, $T$, and end correction length, $\Delta l$, as

$$K_R^{\mathrm{ori}} = \frac{S}{T + \Delta l}. \tag{22}$$

Using Eqs. (21) and (22), the non-dimensional acoustic impedance of an orifice can be expressed as

$$\frac{Z_{\mathrm{ori}}}{M_{\mathrm{ori}}} = \frac{\mathrm{j}k(T+\Delta l)}{M_{\mathrm{ori}}} = \mathrm{j}St'\left(\frac{T}{R_{\mathrm{ori}}} + \frac{\Delta l}{R_{\mathrm{ori}}}\right) = \mathrm{j}St\left(1 + \frac{\Delta l}{T}\right), \tag{23}$$

where $M_{\mathrm{ori}}$ is the Mach number of the mean flow through the orifice and $St = T\omega/U_0$. It is noted that the non-dimensional acoustic impedance in Eq. (23) is expressed by multiplication of the Strouhal number and a term that includes a non-dimensional thickness. Previous results [21–25] reveal that the acoustic impedance of perforated plates with grazing flow can be conveniently non-dimensionalized by the Strouhal number. The orifice radius and the grazing mean flow velocity are major parameters in the grazing flow condition, whereas the orifice thickness and the bias mean flow velocity are dominant in the bias flow condition. In this study, the acoustic impedance is expressed by non-dimensional parameters, viz. $Z_{\mathrm{ori}}/M_{\mathrm{ori}}$, $St$, porosity and $T/R_{\mathrm{ori}}$.

Fig. 3 compares the predicted acoustic impedance given by the present model with the previous impedance models [2,7,9]. The acoustic impedance of a perforated plate for which the thickness-to-radius ratio is 0.5 was predicted with varying porosity from 0.1% to 20%. The modified Howe's model, as suggested by Jing and Sun [7] for consideration of the effect of aperture thickness, is

$$Z_p = Z_e + \mathrm{j}kT, \tag{24}$$

where $Z_e$ denotes the theoretical acoustic impedance of a very thin orifice given by Howe [2] and $Z_p$ implies the modified model for an orifice containing the thickness effect. No appreciable change was observed in the resistance when varying the porosity. However, the gradient of the reactance curve becomes smaller as the porosity increases. When the porosity reaches 0.1%, the predicted reactance is very similar to that of the previous models [2,7,9] that did not consider the interaction effect. When the porosity becomes 20%, the change in the reactance value from that of a single aperture is as much as 30%.

## 3. Experiments

Fig. 4 shows the experimental setup for measuring the acoustic impedance of perforated plates with bias flow. A compressor supplied the airflow through its ancillaries for flow regularization. The flow velocity was measured by a digital flow meter (Flowmetrics FM-20N). The range of mean flow Mach number in the orifice was from 0 to 0.19. The input sound signal was generated by a 200-W compression driver (JBL 2490H)

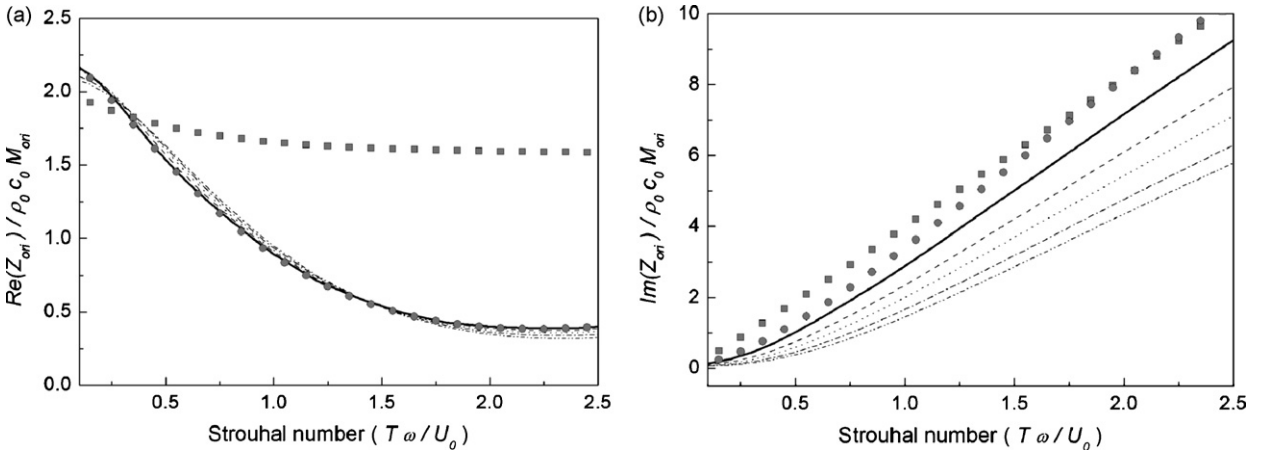


Fig. 3. Predicted acoustic impedance considering the interaction effects ($T/R_{ori} = 0.5$): ▬▬, $\sigma = 0.1\%$; ▬▬, $\sigma = 1.4\%$; ▬ ▬, $\sigma = 5.6\%$; ▪ ▪ ▪ ▪, $\sigma = 9.8\%$; ▬ ▪ ▬, $\sigma = 15\%$; ▬ ▪ ▪ ▬, $\sigma = 20\%$; ■, modified Howe's model [2,7]; ●, Jing and Sun's model [9]. (a) Non-dimensionalized acoustic resistance, (b) non-dimensionalized acoustic reactance.

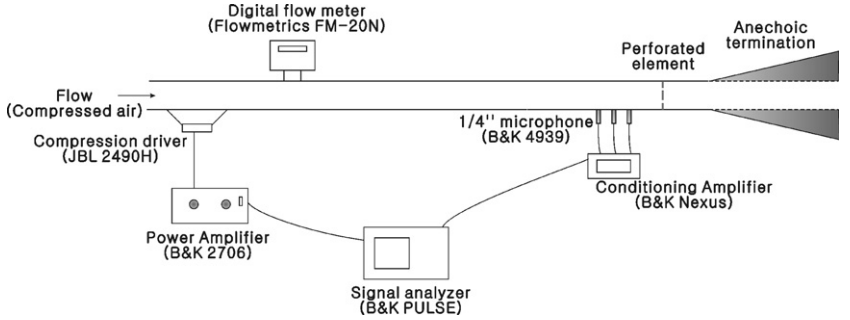


Fig. 4. Experimental setup for measuring the acoustic impedance of perforates with bias flow.

mounted on the upstream side-wall, with a low cutoff frequency of 150 Hz. A swept sine signal was used for exciting the speaker in order to increase the signal-to-noise ratio. A flow meter and a compression driver were installed at 1.5 m upstream to the test section. A square acrylic duct, $30 \times 30\,mm^2$ in cross-section and 10 mm in thickness, was used as the main flow duct. To suppress the negative effect due to reflected sounds, an anechoic termination of the test duct was used. A perforated plate was installed vertically to the main duct. Three quarter-inch microphones (B&K 4939) were flush mounted in series on the upstream duct as an array for reducing errors [26]. The two frequency response functions between microphones were measured and the phase matching was tested before the main experiments. The phase mismatch of the two pairs of microphones and amplifiers were less than 0.5° over the frequency range of the measurements and the remaining small mismatched phase was compensated in the post processing. Generation of source signal and analysis of measured signal were performed by a multichannel signal analyzer (B&K Pulse system). The background noise level in the test duct was less than 48 dB for all frequencies during the experiments. The acoustic impedance of perforates with bias flow was defined by the ratio of the pressure differences between upstream and downstream positions to the particle velocity through perforates. For measuring the impedance of perforated plates with bias flow, the impedance tube method was used [14,27]. The impedance can be obtained by measuring the surface impedance with and without the perforated plate using only upstream mounted microphones. The acoustic impedance under the bias flow condition was measured with the following parameter ranges: $1\,mm \leqslant R_{ori} \leqslant 6.5\,mm$, $0.5\,mm \leqslant T \leqslant 3\,mm$, $5.6\% \leqslant \sigma \leqslant 19.6\%$, $150\,Hz \leqslant f \leqslant 3000\,Hz$, $0.033 \leqslant M_{ori} \leqslant 0.19$, and $100\,dB \leqslant$ in-duct SPL $\leqslant 148\,dB$. It is assumed that the behavior of impedance for input SPLs less than 100 dB would be very similar to those of 100–110 dB. When the bias flow passes through

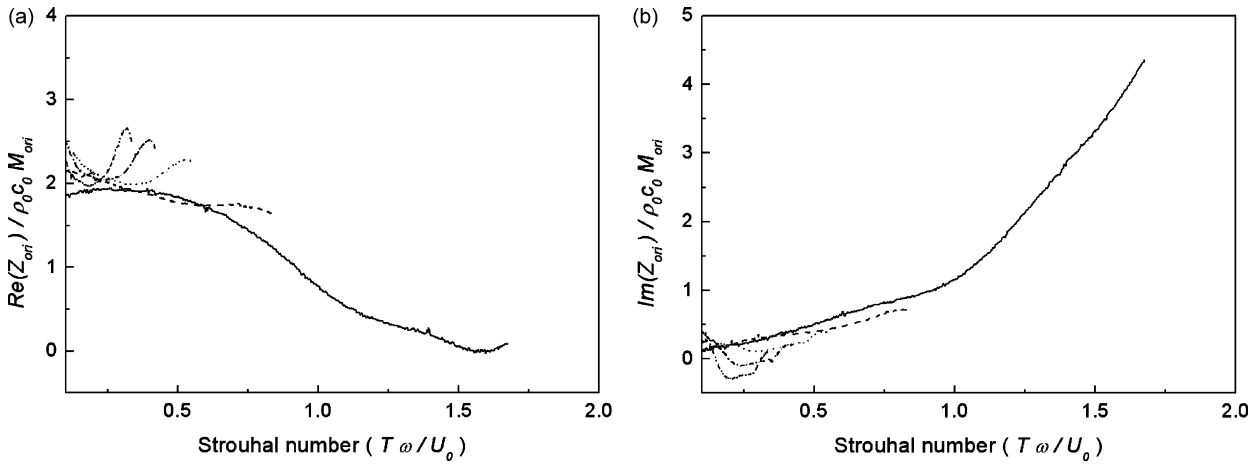


Fig. 5. Measured acoustic impedance with respect to the Strouhal number varying the orifice Mach number ($R_{ori} = 2$ mm, $T = 1$ mm, $\sigma = 20\%$): ——, $M_{ori} = 0.033$; — —, $M_{ori} = 0.066$; - - - - -, $M_{ori} = 0.099$; — - —, $M_{ori} = 0.13$; — - - —, $M_{ori} = 0.17$. (a) Resistance, (b) reactance.

the perforates, the mean flow Mach number of an orifice can be calculated from the mean flow Mach number in the main duct divided by the porosity as given by $M_{ori} = M_{duct}/\sigma$.

Fig. 5 shows the measured acoustic impedance when varying the mean flow Mach number within an orifice. As the mean flow Mach number of an orifice increases, the resistance has peaky values and the reactance experiences sign changes from negative to positive. When the mean flow Mach number of an orifice is larger than about 0.1, a nonlinear trend can be observed. In the next section, where the measured impedance data are compared with predicted values, an orifice Mach number of 0.1 was used because the prediction model in this study does not include such nonlinear effects.

## 4. Comparison of theoretical and experimental results

Before comparison of the measured and predicted results for impedance, the assumptions used in the theoretical model are compared with the actual experimental conditions. The model is based on the following assumptions: the fluid motion is governed by the incompressible Euler equation with high Reynolds number and low Mach number condition; viscous effects are considered only at the rim of aperture, by use of a Kutta condition. Because the incompressibility assumption is reasonable only for slowly time-varying acoustic problems, i.e., at low frequencies, the excitation wavelength should greatly exceed the aperture radius. In the actual experiments, the mean flow Mach number in an orifice ranges from 0.033 to 0.19 and the corresponding Reynolds number in the main duct ranges from 3320 to 24400. The wavelength of the incident wave, which can be determined by the excitation frequency range (150 Hz–3 kHz), varied from 0.113 to 2.27 m and the range of orifice radius was from 0.001 to 0.0065 m. The minimum wavelength of the excitation signal was larger than the maximum orifice radius by a factor of 17.6. Consequently, it can be said that the assumptions in the theoretical model were mostly satisfied in the experiments.

Three major input parameters are required for the numerical predictions: the Strouhal number, the ratio of orifice thickness to orifice radius, and the ratio of tube radius to orifice radius. The radius ratio of tube to orifice can be expressed solely in terms of the porosity, as

$$R_{tub}/R_{ori} = \sqrt{S_{pla}/n\pi}\Big/R_{ori} = 1/\sqrt{\sigma}, \tag{25}$$

where $S_{pla}$ denotes the area of perforated plate and $n$ is the number of orifices. In Figs. 6 and 7, measured and predicted acoustic impedance values are compared for the same thickness-to-radius ratio ($T/R_{ori} = 1$ for Fig. 6 and $T/R_{ori} = 1.5$ for Fig. 7) and porosity ($\sigma = 15.4\%$). They show reasonable agreement in the low Strouhal number region, especially for reactance. The trend in resistance is reasonable but the deviation was about

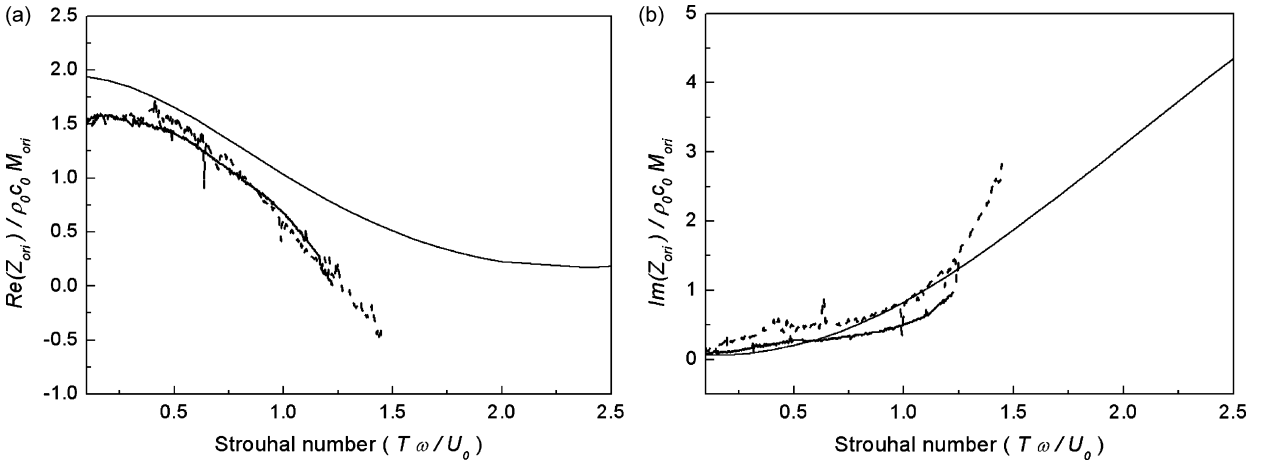


Fig. 6. A comparison of measured and predicted acoustic impedance of perforated plates having same thickness-to-radius ratio and porosity: ▬▬, measured ($T/R_{ori}$ ( = 1.5 mm/1.5 mm) = 1, $\sigma = 15.4\%$); ▬ ▬, measured ($T/R_{ori}$ ( = 2 mm/2 mm) = 1, $\sigma = 15.4\%$); ———, predicted ($T/R_{ori} = 1$, $\sigma = 15.4\%$). (a) Resistance, (b) reactance.

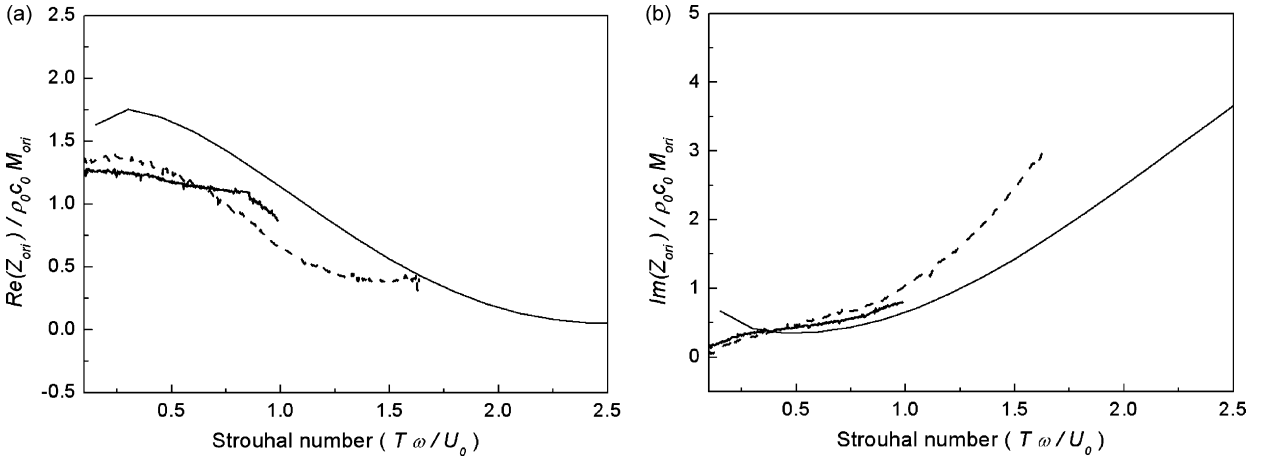


Fig. 7. A comparison of measured and predicted acoustic impedance of perforated plates having same thickness-to-radius ratio and porosity: ▬▬, measured ($T/R_{ori}$ ( = 1.5 mm/1 mm) = 1.5, $\sigma = 15.4\%$); ▬ ▬, measured ($T/R_{ori}$ ( = 3 mm/2 mm) = 1.5, $\sigma = 15.4\%$); ———, predicted ($T/R_{ori} = 1.5$, $\sigma = 15.4\%$). (a) Resistance, (b) reactance.

10–20% for $St = 0$–1.3. As the Strouhal number increases, discrepancies in the reactance increase. When the ratio of thickness-to-radius is large, a similar trend holds for the measured and predicted acoustic impedance. Fig. 8 shows a comparison of measured and predicted impedance when the porosity varies from 5.6% to 19.6% ($R_{ori} = 2$ mm, $T = 1$ mm). Measured and predicted reactance increase slowly with increasing porosity. The change of acoustic impedance with varying ratio of thickness-to-radius is shown in Figs. 9 and 10. Fig. 9 illustrates the effects of this ratio on the acoustic impedance as the orifice radius varies from 1.5 to 6.5 mm, with fixed thickness and porosity ($T = 1.5$ mm, $\sigma = 15.4\%$). Fig. 10 shows the effect of the ratio as the orifice thickness varies from 1 to 3 mm, with fixed orifice radius and porosity ($R_{ori} = 2$ mm, $\sigma = 15.4\%$). In the foregoing results, the predicted acoustic impedance considering interaction effects shows reasonable agreement with measurements. However, the experimental results indicate little change of reactance with thickness-to-radius ratio as the thickness changes, but a large effect similar to the predicted values as the radius changes. The reactance tends to increase as the thickness-to-radius ratio decreases because the attached mass increases.

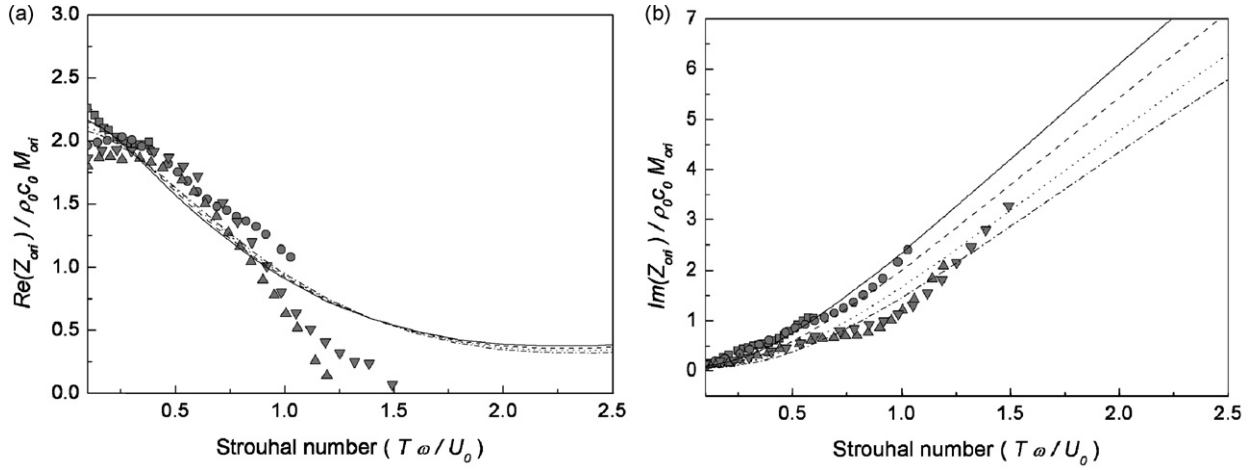


Fig. 8. A comparison of measured and predicted acoustic impedance varying the porosity ($R_{ori} = 2$ mm, $T = 1$ mm): ▬▬, $\sigma = 5.6\%$ (predicted); — —, $\sigma = 9.8\%$ (predicted); - - - - -, $\sigma = 15.4\%$; ▬ - ▬, $\sigma = 19.5\%$ (predicted); ■, $\sigma = 5.6\%$ (measured); ●, $\sigma = 9.8\%$ (measured); ▲, $\sigma = 15.4\%$ (measured), $\sigma = 19.5\%$ (measured). (a) Resistance, (b) reactance.

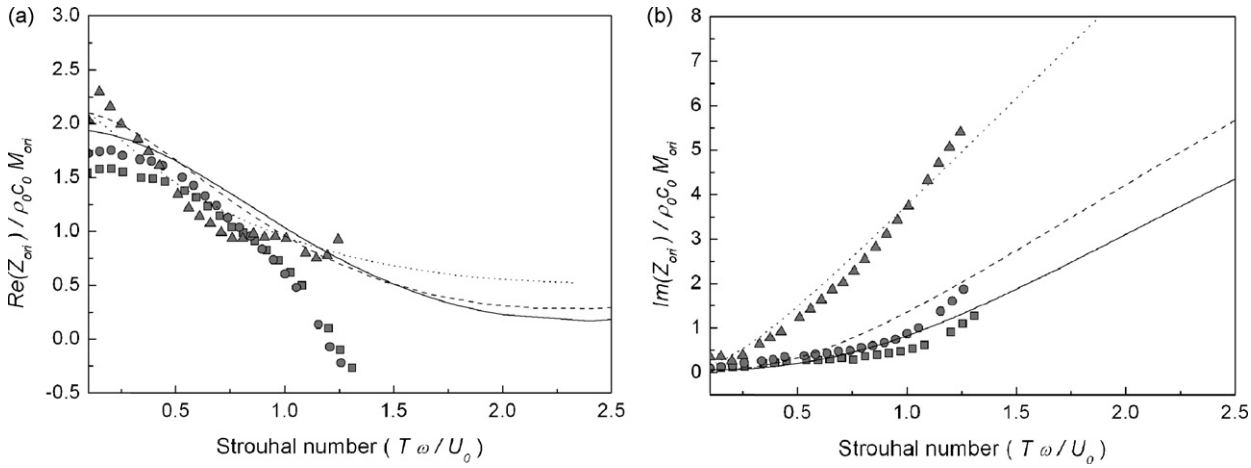


Fig. 9. A comparison of measured and predicted acoustic impedance varying the thickness-to-radius ratio ($\sigma = 15.4\%$, $T = 1.5$ mm): ▬▬, $T/R_{ori} = 1$ (predicted); — —, $T/R_{ori} = 0.6$ (predicted); - - - - -, $T/R_{ori} = 0.23$ (predicted); ■, $T/R_{ori} = 1$ (measured); ●, $T/R_{ori} = 0.6$ (measured); ▲, $T/R_{ori} = 0.23$ (measured). (a) Resistance, (b) reactance.

In order to verify the effect of interaction between orifices, the transmission loss of perforated baffles under bias flow conditions was also measured and predicted. The experimental setup for measuring the transmission loss of a perforated plate under bias flow conditions was very similar to that shown in Fig. 4, except that another three microphone array was used downstream of the perforated baffle. A perforated plate, $30 \times 30\,mm^2$ in size, 1 mm in thickness, with orifices of 2 mm in diameter, was used in all experiments, with varying porosity. The transmission loss was obtained by using downstream and upstream reflection coefficients and the transfer function between two microphones located upstream and downstream of the test section [28]. For the prediction of transmission loss, the four pole parameters of a perforated plate were used. Fig. 11 shows a comparison between measured and predicted transmission loss. The predicted transmission loss from the new model that considers orifice interactions shows better agreement with measured data than that by the other two models which ignore the interaction effect. From this result, it is seen that consideration of the interaction effect between orifices is important in the prediction of the acoustic performance of silencing devices that contain perforated elements with bias flow.

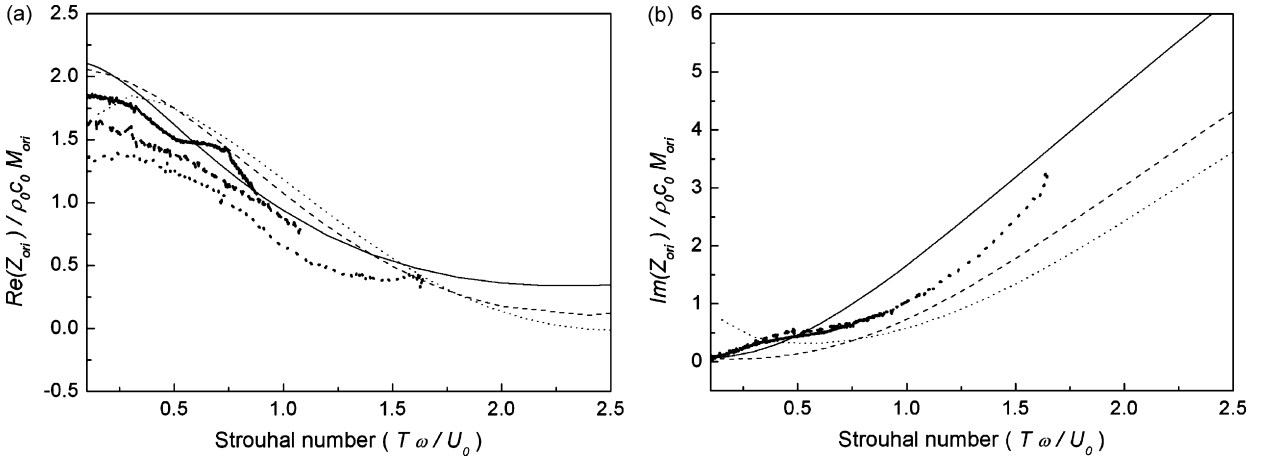


Fig. 10. A comparison of measured and predicted acoustic impedance varying the thickness-to-radius ratio ($\sigma = 15.4\%$, $R_{ori} = 2$ mm): ——, $T/R_{ori} = 0.5$; — —, $T/R_{ori} = 1$; - - - - -, $T/R_{ori} = 1.5$; thick lines, measured; thin lines, predicted. (a) Resistance, (b) reactance.

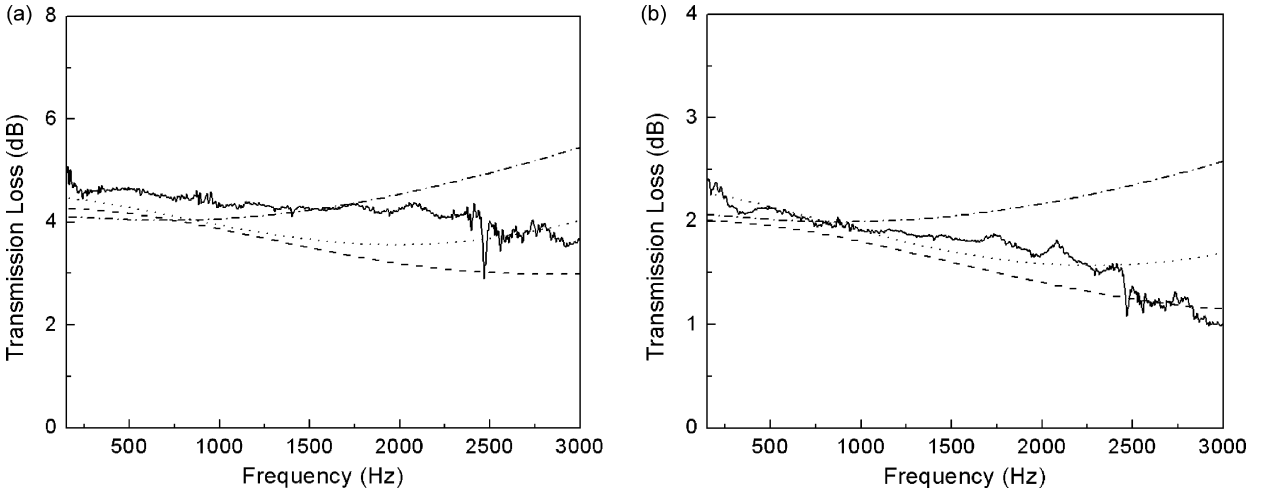


Fig. 11. A comparison of measured and predicted transmission loss of perforated plate considering the interaction effect ($R_{ori} = 2$ mm, $T = 1$ mm): ——, measured; — —, present model; - - - - -, Jing and Sun's model [9]; — - —, modified Howe's model [2,7]. (a) $\sigma = 9.8\%$, $M_{ori} = 0.06$; (b) $\sigma = 20\%$, $M_{ori} = 0.05$.

## 5. Conclusions

In this study, the effect of interaction between orifices on the acoustic impedance of perforated plates with bias flow was analyzed numerically and experimentally. In the numerical predictions, the acoustic impedance of an orifice of radius $R_{ori}$ in a finite-thickness partition across a tube of radius $R_{tub}$ was calculated by solving the incompressible Euler equation using the boundary-element method. The analysis implies that the acoustic impedance, in the form of the normalized impedance of an orifice divided by the mean flow Mach number through an orifice, $Z_{ori}/M_{ori}$, is governed by a further three non-dimensional parameters. These are the porosity, the thickness-to-radius ratio and the Strouhal number, defined as $T\omega/U_0$. The measurements were repeated with varying orifice diameter, orifice thickness, porosity, and mean flow Mach number through an orifice. Nonlinear trends in both resistance and reactance were observed in the measurements when the mean flow Mach number through an orifice exceeded 0.1. Measured and predicted acoustic impedance were compared for varying porosity and thickness-to-radius ratio. As the porosity increases, the reactance tends to

decrease because of the interaction between orifices. The predicted impedance considering the interaction effect showed reasonable agreements with measured data over the range of porosity used in the experiments, namely 5–20%. Calculated orifice impedance values were used to predict the transmission loss of a perforated baffle partition in a tube with bias flow. Within the frequency range that satisfies the incompressibility assumption, viz., for frequencies at which the excitation wavelength far exceeds the aperture radius, the predicted values were compared with measured transmission loss results and the present model was shown to be better than the previous models, especially for results at the high end of the frequency range.

## Acknowledgments

This work was partially supported by the BK21 Project.

## References

[1] A.B. Bauer, Impedance theory and measurements on porous acoustic liners, *Journal of Aircraft* 14 (1977) 720–728.
[2] M.S. Howe, On the theory of unsteady high Reynolds number flow through a circular aperture, *Proceedings of the Royal Society A* 366 (1979) 205–223.
[3] D.W. Bechert, Sound absorption caused by vorticity shedding, demonstrated with a jet flow, *Journal of Sound and Vibration* 70 (1980) 389–405.
[4] I.J. Hughes, A.P. Dowling, The absorption of sound by perforated linings, *Journal of Fluid Mechanics* 218 (1990) 299–335.
[5] M.S. Howe, Influence of wall thickness on Rayleigh conductivity and flow-induced aperture tones, *Journal of Fluids and Structures* 11 (1997) 351–366.
[6] K.S. Peat, R. Sugimoto, J.L. Horner, The effects of thickness on the impedance of a rectangular aperture in the presence of a grazing flow, *Journal of Sound and Vibration* 292 (2006) 610–625.
[7] X.D. Jing, X.F. Sun, Experimental investigations of perforated liners with bias flow, *Journal of the Acoustical Society of America* 106 (1999) 2436–2441.
[8] J.W.S. Rayleigh, *Theory of Sound*, Vol. II, Dover, New York, 1945 (Section 306).
[9] X.D. Jing, X.F. Sun, Effect of plate thickness on impedance of perforated plates with bias flow, *AIAA Journal* 38 (2000) 1573–1578.
[10] V. Bellucci, C.O. Paschereit, P. Flohr, Impedance of perforated screen with bias flow, *AIAA Paper 2002-2437*, 2002.
[11] J.D. Eldredge, A.P. Dowling, The absorption of axial acoustic waves by a perforated liner with bias flow, *Journal of Sound and Vibration* 485 (2003) 307–335.
[12] P.D. Dean, A.P. Tester, Duct wall impedance control as an advanced concept for acoustic suppression, *NASA CR-134998*, 1975.
[13] M. Salikuddin, A.A. Syed, P. Mungur, Acoustic characteristics of perforated sheets with throughflow in a high-intensity noise environment, *Journal of Sound and Vibration* 169 (1994) 145–177.
[14] U. Ingard, On the theory and design of acoustic resonators, *Journal of the Acoustical Society of America* 25 (1953) 1037–1061.
[15] V.A. Fok, *Doklady Akademii nauk SSSR* 31 (1941). (in Russian) Alternatively, see S.N. Rschevkin, *A Course of Lectures on the Theory of Sound*, Pergamon Press, London, 1963 (Chapter VII).
[16] T.H. Melling, The acoustic impedance of perforates at medium and high sound pressure levels, *Journal of Sound and Vibration* 29 (1973) 1–65.
[17] I.G. Currie, *Fundamental Mechanics of Fluids*, McGraw-Hill, Inc., New York, 1993 (Chapter 3).
[18] H. Rouse, A. Abul-Fetouh, Characteristics of irrotational flow through axially symmetric orifices, *Journal of Applied Mechanics* 17 (1950) 421–426.
[19] B.W. Hunt, Numerical solution of an integral equation for flow from a circular orifice, *Journal of Fluid Mechanics* 31 (1968) 361–377.
[20] L.C. Wrobel, M.H. Aliabadi, *The Boundary Element Method*, Vol. I, Wiley, New York, 2002 (Chapter 2).
[21] J.W. Kooi, S.L. Sarin, An experimental study of the acoustic impedance of Helmholtz resonator arrays under a turbulent boundary layer, *AIAA Paper 81-1998*, 1981.
[22] A. Cummings, The effects of grazing turbulent pipe-flow on the impedance of an orifice, *Acoustica* 61 (1986) 233–242.
[23] R. Kirby, A. Cummings, The impedance of perforated plates subjected to grazing gas flow and backed by porous media, *Journal of Sound and Vibration* 217 (1998) 619–636.
[24] S.-H. Lee, J.-G. Ih, Empirical model of the acoustic impedance of a circular orifice in grazing mean flow, *Journal of the Acoustical Society of America* 114 (2003) 98–113.
[25] K.S. Peat, J.-G. Ih, S.-H. Lee, The acoustic impedance of a circular orifice in grazing mean flow: comparison with theory, *Journal of the Acoustical Society of America* 114 (2003) 3076–3086.
[26] S.-H. Jang, J.-G. Ih, On the multiple microphone method for measuring in-duct acoustic properties in the presence of mean flow, *Journal of the Acoustical Society of America* 103 (1998) 1520–1526.
[27] K.H. Rao, M.L. Munjal, Experimental evaluation of impedance of perforate with grazing flow, *Journal of Sound and Vibration* 108 (1986) 283–295.
[28] J.Y. Chung, D.A. Blaser, Transfer function method of measuring in-duct acoustic properties. I. Theory, *Journal of the Acoustical Society of America* 68 (1980) 907–913.